

The *NGATHA* Genes Direct Style Development in the *Arabidopsis* Gynoecium

Marina Trigueros,^{a,1} Marisa Navarrete-Gómez,^{a,1} Shusei Sato,^b Sioux K. Christensen,^c Soraya Pelaz,^{b,d} Detlef Weigel,^{c,e} Martin F. Yanofsky,^b and Cristina Ferrándiz^{a,b,2}

^a Instituto de Biología Molecular y Celular de Plantas, Universidad Politécnica de Valencia, Consejo Superior de Investigaciones Científicas, 46022 Valencia, Spain

^b Section of Cell and Developmental Biology, University of California at San Diego, La Jolla, California 92093

^c Plant Biology Laboratory, The Salk Institute for Biological Studies, La Jolla, California 92037

^d Institució Catalana de Recerca i Estudis Avançats and Centre for Research in Agricultural Genomics, 08034 Barcelona, Spain

^e Department of Molecular Biology, Max Planck Institute for Developmental Biology, 72076 Tübingen, Germany

The gynoecium is the most complex floral organ, designed to protect the ovules and ensure their fertilization. Correct patterning and tissue specification in the developing gynoecium involves the concerted action of a host of genetic factors. In addition, apical-basal patterning into different domains, stigma and style, ovary and gynophore, appears to depend on the establishment and maintenance of asymmetric auxin distribution, with an auxin maximum at the apex. Here, we show that a small subfamily of the B3 transcription factor superfamily, the *NGATHA* (*NGA*) genes, act redundantly to specify style development in a dosage-dependent manner. Characterization of the *NGA* gene family is based on an analysis of the activation-tagged mutant named *tower-of-pisa1* (*top1*), which was found to overexpress *NGA3*. Quadruple *nga* mutants completely lack style and stigma development. This mutant phenotype is likely caused by a failure to activate two auxin biosynthetic enzymes, *YUCCA2* and *YUCCA4*, in the apical gynoecium domain. The *NGA* mutant phenotypes are similar to those caused by multiple combinations of mutations in *STYLISH1* (*STY1*) and additional members of its family. *NGA3/TOP1* and *STY1* share almost identical patterns of expression, but they do not appear to regulate each other at the transcriptional level. Strong synergistic phenotypes are observed when *nga3/top1* and *sty1* mutants are combined. Furthermore, constitutive expression of both *NGA3/TOP1* and *STY1* induces the conversion of the ovary into style tissue. Taken together, these data suggest that the *NGA* and *STY* factors act cooperatively to promote style specification, in part by directing *YUCCA*-mediated auxin synthesis in the apical gynoecium domain.

INTRODUCTION

The last two decades have seen substantial advances in our knowledge of the molecular genetics directing floral meristem and organ identity development, leading to a clear picture of how floral organ identity is acquired (Robles and Pelaz, 2005). Once organ identity is established; however, different tissues must differentiate in the correct pattern to ensure organ function, and we are only now beginning to understand the genetic pathways directing floral organ patterning.

The gynoecium, the female reproductive structure from which fruits derive, is the most complex floral organ. In *Arabidopsis thaliana*, the gynoecium comprises two congenitally fused carpels that arise from the floral meristem forming a hollow cylinder.

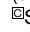
Subsequently, apical-basal, adaxial-abaxial, and radial patterns are established and distinct tissues differentiate sequentially. Along the apical-basal axis, the mature *Arabidopsis* gynoecium consists of a short basal, stem-like structure, the gynophore, on top of which a bilocular ovary forms, capped with a solid style and stigmatic papillae (Figure 1A). In the transversal plane, three major regions can be distinguished: the valves, which correspond to the two carpel walls, and the valve margins and the replum in the zones of carpel fusion (Figure 1A). Meristematic tissues are present in the carpel margins, which give rise to the apical style and stigma, and the internal septum, transmitting tract and ovule producing placenta on the adaxial side of the gynoecium (Ferrándiz et al., 1999; Balanza et al., 2006). Most of the tissues that make up these regions in the gynoecium can be distinguished functionally and/or morphologically, and several mutants that specifically affect subsets of these tissues have been identified (Balanza et al., 2006).

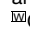
The genetic networks underlying differentiation of valves, valve margins, and replum have been extensively studied in the last few years, leading to the proposal of a well-supported and detailed model for patterning on the transversal plane of the ovary (Dinneny and Yanofsky, 2005; Alonso-Cantabrana et al., 2007). Similarly, a number of mutants affecting the distribution of tissues along the apical-basal axis of the gynoecium have been

¹ These authors contributed equally to this work.

² Address correspondence to cferrandiz@ibmcp.upv.es.

The author responsible for distribution of materials integral to the findings presented in this article in accordance with the policy described in the Instructions for Authors (www.plantcell.org) is: Cristina Ferrándiz (cferrandiz@ibmcp.upv.es).

 Some figures in this article are displayed in color online but in black and white in the print edition.

 Online version contains Web-only data.

www.plantcell.org/cgi/doi/10.1105/tpc.109.065508

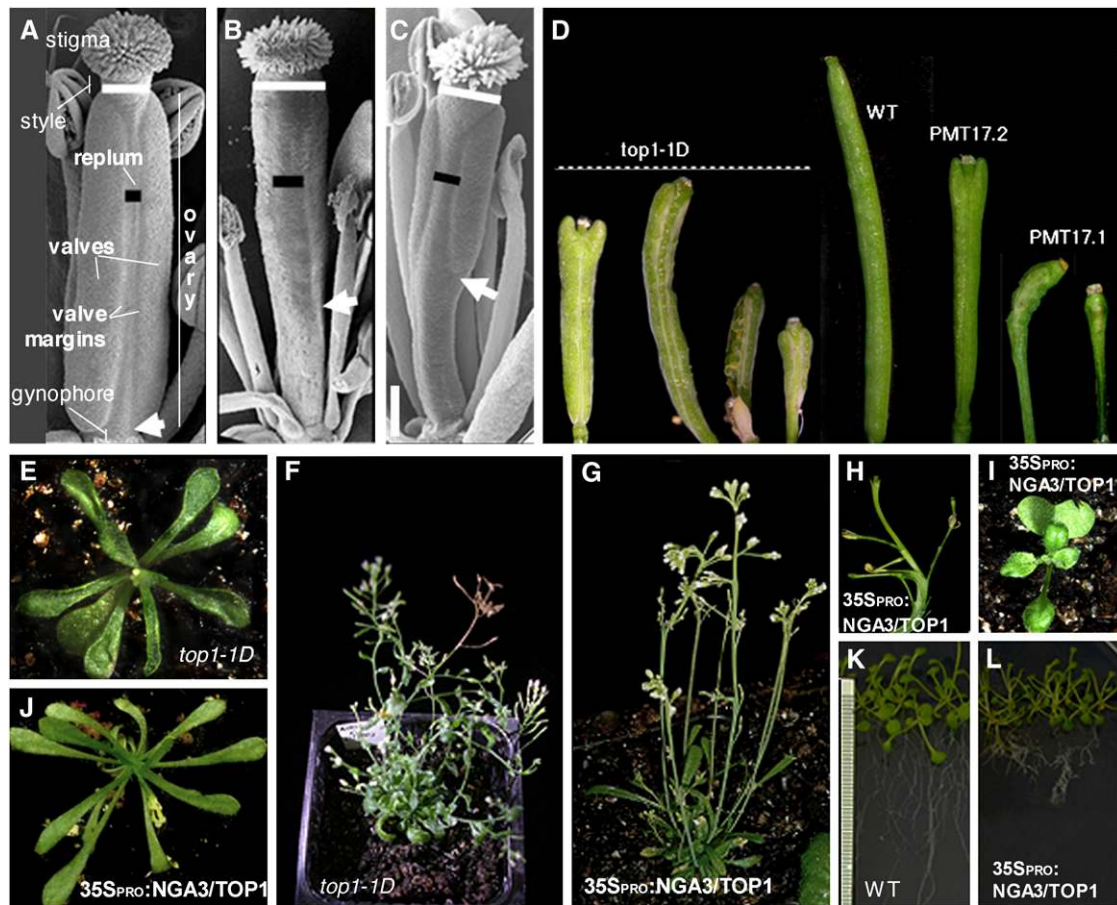


Figure 1. Phenotypes Caused by Ectopic Expression of *NGA3/TOP1*.

(A) to (C) Scanning electron micrographs of anthesis gynoecia from the wild type (A), *top1-1D* (B), and *35S_{PRO}:NGA3* (C). The different regions of the anthesis gynoecium are indicated in (A). Arrows mark the valve-gynophore boundary, black horizontal bars indicate the width of the replum, and white horizontal bars indicate the width of the style. Bars = 200 μ m.

(D) Comparison of mature siliques from the *top1-1D* mutant (left), the wild type (center), and two independent *35S_{PRO}:NGA3* lines (right), where PMT17.2 is representative of an intermediate phenotype and PMT17.1 of a strong phenotype.

(E) and (J) Rosette morphology of *top1-1D* (E) and *35S_{PRO}:NGA3* (J) lines, 20 d after sowing.

(F) and (G) Plant architecture phenotypes of *top1-1D* (F) and *35S_{PRO}:NGA3* lines (G), 5 weeks after sowing.

(H) Fasciation of the stem in a *35S_{PRO}:NGA3* inflorescence.

(I) Partially fused cotyledons of a *35S_{PRO}:NGA3* young plant.

(K) and (L) Root morphology of wild-type Col (K) and *35S_{PRO}:NGA3* lines (L) grown for 6 d in vertical Murashige and Skoog plates.

identified, but their regulatory hierarchies or their mechanisms of action are much less understood. A major factor for the differentiation of the apical tissues of the gynoecium is the *SPATULA* (*SPT*) gene, which encodes a basic helix-loop-helix transcription factor (Heisler et al., 2001). *spt* mutant gynoecia have reduced style and stigmatic tissues, are partially unfused at the apical end, and lack transmitting tract development (Alvarez and Smyth, 1999). *SPT* protein is able to interact with the HECATE basic helix-loop-helix proteins, three related factors that redundantly participate in stigma, septum, and transmitting tract development (Gremski et al., 2007). *STYLISH1* (*STY1*), *STY2*, and other members of the small SHI-like gene family of RING-finger transcription factors also direct apical tissue formation, as

revealed by the partial loss of style and stigma caused by mutations in *STY1* and related genes or the ectopic development of patches of style-like tissue in the valves of plants overexpressing *STY1* (Kuusk et al., 2002, 2006). Somewhat opposite phenotypes to *spt* or *sty* multiple mutants are seen when *ETTIN* (*ETT*)/*AUXIN RESPONSE FACTOR3* is mutated. *ett* mutants show severe defects in apical-basal patterning, with an increase of the apical and basal regions (style/stigma and gynophore, respectively) and a decrease in the size of the ovary (Sessions and Zambryski, 1995; Sessions et al., 1997; Pekker et al., 2005). The regulatory hierarchies of these factors are only partially known. Genetic analyses have placed *STY1* and related genes downstream of *SPT*, although the precise molecular

mechanisms are not known (Groszmann et al., 2008; Staldal et al., 2008). Likewise, it appears that *ETT* restricts *SPT* expression to the apical domain and that ectopic expression of *SPT* is largely responsible for the apical-basal patterning defects in *ett* mutants (Heisler et al., 2001).

Together with these genetic factors, auxin appears to play a key role in the specification of the different domains along the apical-basal axis of the *Arabidopsis* gynoecium. This was first suggested by the phenotypes of mutants affecting auxin transport or signaling. Several of these mutants show defects in apical-basal patterning, with an increase of the apical and basal regions (style/stigma and gynophore, respectively) and a decrease in the size of the ovary (Okada et al., 1991; Bennett et al., 1995; Sessions et al., 1997). Second, gynoecia treated with polar-auxin-transport inhibitors exhibit very similar defects, leading Nemhauser et al. (2000) to propose a model where the apical-basal patterning is dependent on an auxin gradient spanning the gynoecial primordium with peak levels in the apical regions and descending levels basally. According to this hypothesis, high auxin levels would promote proliferation of style and stigma; intermediate levels the ovary and low levels the gynophore. Inhibition of auxin transport in the gynoecium would lead to auxin accumulation in source tissues, hypothesized to be the apical parts, and depletion in the basal regions, which is in agreement with the observed effects (Nemhauser et al., 2000). The *YUCCA* (*YUC*) genes encode flavin monooxygenases involved in auxin biosynthesis. Two of the 11 *Arabidopsis* *YUC* genes, *YUC2* and *YUC4*, are expressed in the apical gynoecium, and multiple *yuc* mutants exhibit a strongly affected gynoecium patterning, supporting the proposed key role of auxin synthesis in the apical domains to direct gynoecium morphogenesis (Cheng et al., 2006). This hypothesis has received further support by the finding that *STY1* activates *YUC4* expression (Sohlberg et al., 2006) and the restoration of *sty1 sty2* defects in apical gynoecium development by exogenous application of auxin (Staldal et al., 2008).

Our understanding of the genetic networks directing apical-basal patterning in the gynoecium has increased greatly in the last few years, although the current models that explain the underlying molecular mechanisms are not as complete as for the transversal plane of the ovary. Among other reasons, it is likely that other gene functions influencing this process have yet to be identified. Among those, there may be highly redundant genes, whose functions are difficult to reveal through traditional mutant screening approaches. This work describes the functional characterization of four highly related genes that promote the formation of apical tissues during carpel development, the *NGATHA* (*NGA*) genes. We identified *NGA3/TOP1*, in an activation tagging mutagenized population (Weigel et al., 2000), by the severe phenotype observed in gynoecium development caused by *NGA3/TOP1* overexpression. We then used a reverse genetics approach to obtain loss-of-function mutants in *NGA3/TOP1* and three closely related homologs, *NGA4*, *NGA2*, and *NGA1*. The *NGA* genes act redundantly to promote apical tissue development in the *Arabidopsis* gynoecium. We present data based on genetic analyses that indicate that the *NGA* genes act in parallel with the *STY* genes to direct style development, partially through activation of *YUC*-mediated auxin synthesis in the apical gynoecium.

RESULTS

Phenotypic Defects of the Activation Tagging Mutant *top1-1D*

To identify genes involved in carpel and fruit development in *Arabidopsis*, we screened a population derived from an activation-tagging mutagenesis, in which cauliflower mosaic virus (CaMV) 35S transcriptional enhancers are randomly integrated into the genome. We identified a putative mutant among the primary transformants, which we named *tower-of-pisa1-1D* (*top1-1D*), which showed elongation and patterning defects in silique development (Weigel et al., 2000). This line had very reduced self-fertility; therefore, we outcrossed it to wild-type Columbia (Col) plants to test for heritability of the phenotype in the progeny. The original phenotype was reproduced in approximately three-quarters of the progeny, as expected for a dominant mutation, and cosegregated with herbicide resistance encoded by the activation tagging vector, but showed different degrees of expressivity.

The *top1-1D* plants had severely affected fruit size and shape. The *top1-1D* phenotypes were highly variable even within the same plant: the strongest phenotypes corresponded to fruits with reduced valve size, long gynophores, and enlarged styles (Figure 1B); other fruits showed an abnormal replum morphology (Figures 1B and 1D); finally, aberrant shapes were also found, most frequently an outgrowth of the tip of the valves to produce fruit with the shape of an inverted arrow head (Figure 1D). *top1-1D* plants also showed pleiotropic phenotypes that affected root growth, leaf morphology (Figure 1E), and inflorescence development (Figure 1F), as well as a high rate of mortality before completing the reproductive cycle. The expressivity of these phenotypes was found to be highly variable and rapidly lost in subsequent generations, probably due to silencing of the CaMV 35S enhancer. Therefore, we did not perform a more detailed phenotypic characterization of this line.

top1-1D Mutants Overexpress the *NGA3* Gene Encoding a B3 DNA Binding Protein

The *top1-1D* line was found to contain a single insertion of the activation tagging T-DNA. Plasmid rescue was performed, and we determined the site of insertion in a region covered by BAC T25K16 in chromosome 1. An open reading frame (ORF) annotated as a B3 DNA binding domain protein (At1g01030) was found 2654 bp downstream of the 4x35S enhancer of the T-DNA (see Supplemental Figure 1A online). We found the corresponding RNA to be strongly upregulated in *top1-1D* inflorescences compared with the wild type, where it was detected only at low levels (see Supplemental Figure 1D online). At1g01030 has been described in the literature as *NGA3*, which is part of a small gene family having four members (*NGA1* to *NGA4*; Alvarez et al., 2006). To further confirm that the observed phenotypes were caused by ectopic *NGA3* expression, we transformed wild-type Col-0 plants with two different constructs. CFM97 consisted of a 5.2-kb *EcoRI-PstI* genomic fragment spanning a region containing the *NGA3* ORF placed after a tandem repeat of the CaMV 35S promoter in a pBIN19 vector backbone (35SX2_{PRO}:*NGA3*). The 35SX2_{PRO}:

NGA3 lines showed phenotypes similar to *top1-1D* mutants; moreover, these lines also behaved similarly in the gradual phenotypic attenuation in subsequent generations. To overcome this effect, we generated a new construct, pMT17 (35S_{PRO}:NGA3), where the NGA3 ORF was placed after a single copy of the CaMV 35S promoter in a pGREENII vector backbone. Nine out of 12 35S_{PRO}:NGA3 T1 transgenic lines showed abnormal leaf morphology: rosette leaves were long and narrow and of darker color, similar to those observed in *top1-1D* lines (Figure 1J). Three of them developed carpels with the inverted arrow morphology found in the attenuated *top1-1D* lines, while two other lines showed the strong carpel development defects initially found in the *top1-1D* line: long gynophores, enlarged repla, and reduced valves (Figures 1C and 1D). In addition to their major effect in gynoecium patterning, 35S_{PRO}:NGA3 strong lines showed pleiotropic phenotypes that affected most phases of vegetative and reproductive development. Approximately 20% of the 35S_{PRO}:NGA3 seedlings showed altered cotyledon development, with either fused or cup-shaped cotyledons (Figure 1I). Roots of 35S_{PRO}:NGA3 plants were frequently short and showed a higher proliferation of secondary roots, similar to those grown in the presence of exogenous auxin (Figure 1L). The 35S_{PRO}:NGA3 plants had reduced apical dominance and altered flower phyllotaxy, with frequent fasciation of the stem (Figures 1G and 1H). All these phenotypes have been previously associated with either altered auxin homeostasis or signaling (Bennett et al., 1995). The 35S_{PRO}:NGA3 strong phenotypes were maintained in subsequent generations; therefore, this line could be used for genetic analysis.

Identification of *nga3/top1* Loss-of-Function Mutants

To gain further insight into NGA3/TOP1 gene function, we identified loss-of-function *nga3/top1* mutants in publicly available insertion collections. Two alleles of NGA3/TOP1 from the AMAZE transposon-tagged population (Wisman et al., 1998) and one in the SAIL collection (Sessions et al., 2002) were isolated by reverse genetics in the Col-0 genetic background (see Supplemental Figure 1B online). The strongest phenotypes corresponded to the *nga3-3* allele, where a 600-bp nontransposable fragment of the En-1 element is located in the second exon at position 404 (see Supplemental Figure 1B online). Homozygous *nga3-3* mutant plants showed variable phenotypic effects, affecting only gynoecium development. A variable fraction of the fruits of each plant showed defects in their apical domain. Most frequent were fruit with long and narrow styles, where valve growth was slightly unequal at the top, causing the style to be tilted to one side, hence the original “Tower of Pisa” name (Figures 2A, 2B, 2F, and 2G). Occasionally, fruit showed more severe phenotypes, with an incomplete fusion of the upper region of the carpel that caused a reduced stigma, an abnormal split style, and reduced fertility (Figure 2G). These severe phenotypes were apparent from early stages of development (see Supplemental Figure 2 online). *nga3-1* has a T-DNA insertion at position 221, and *nga3-2* has a En-Spm element inserted at position 861 of the NGA3 ORF. Both *nga3-1* and *nga3-2* plants exhibited only a subtle phenotype of long and narrow styles (Figure 2H), and only at low frequency (<2%) were tilted styles or open gynoecia found.

NGA1, NGA2, and NGA4 Are Related Genes with Similar Function to NGA3/TOP1

Database search analysis revealed three close NGA3/TOP1 homologs in the *Arabidopsis* genome. The four related genes define a subgroup in the RAV family of the B3 superfamily of transcription factors (Swaminathan et al., 2008) and were described previously by Alvarez et al. (2006) as NGA1-NGA4. The most similar to NGA3/TOP1 is NGA4 (41% identity in predicted amino acid sequence), followed by NGA2 (37% identity) and NGA1 (37% identity), with NGA2 and NGA1 being more similar to each other (58% identity).

We identified two insertions in NGA4 in the AMAZE collection, where the En-1 element was inserted at positions –95 (*nga4-2*) and 125 bp (*nga4-3*), respectively, of the NGA4 coding region (see Supplemental Figure 1B online). These mutations caused phenotypes related to those found in *nga3/top1* mutants, fully penetrant, but subtle, affecting style morphology. The styles of both mutant lines were longer and narrower than the wild type, and only occasionally, slightly tilted styles developed, with a stronger effect of the second allele (Figures 2C and 2I). An additional insertion mutant, named *nga2-2*, was identified for NGA2. *nga2-2* mutants had an En-1 element inserted in position 572, which prevented full-length NGA2 RNA accumulation (see Supplemental Figure 1C online) but did not cause clear phenotypic alterations in gynoecium development or elsewhere (Figures 2D and 2J). No insertions were found in the NGA1 coding region, but a line was identified, named *nga1-4*, in which a T-DNA was inserted 171 bp downstream of the stop codon of NGA1 exhibited a significant reduction in NGA1 mRNA levels but had no obvious phenotypic effects other than causing slightly longer styles at low frequency (Figure 2K; see Supplemental Figure 1C online).

Transgenic lines expressing NGA2, NGA3, or NGA4 under the control of the CaMV 35S promoter showed phenotypes similar to those caused by ectopic expression of NGA3 (see Supplemental Figure 3A online). The sequence similarity and the resemblance of both the loss-of-function and the overexpression phenotypes suggested that the four NGA genes could be regulating the same processes. To uncover possible functional redundancy, we characterized double, triple, and quadruple mutants. All double combinations tested showed stronger defects in gynoecium development, especially those containing the *nga3-3* allele. Double mutant combinations with *nga3-3* together with *nga1*, *nga2*, or *nga4* caused most gynoecia to show severe defects in style and stigma development. Double mutant plants showed variable phenotypic expressivity, ranging from completely unfused carpels with poor style or stigma development to mild defects in apical gynoecium development similar to the typical tilted styles of *nga3-3* single mutants (Figures 2L to 2O). The most striking phenotypes were observed in triple and quadruple mutants in which all carpels were completely unfused at the apical end, terminating in serrated structures with no apparent style or stigma development (Figures 2P to 2R). Dose-dependent function of the four NGA activities was further suggested by the long narrow and occasionally tilted styles found in quadruple heterozygotes (*nga1-4/+ nga2-2/+ nga3-3/+ nga4-3/+*; Figure 2E). In addition to defects in gynoecium morphology, triple and quadruple mutants developed enlarged serrated leaves and flowered slightly later than the wild type (see Supplemental Figure 3B online).

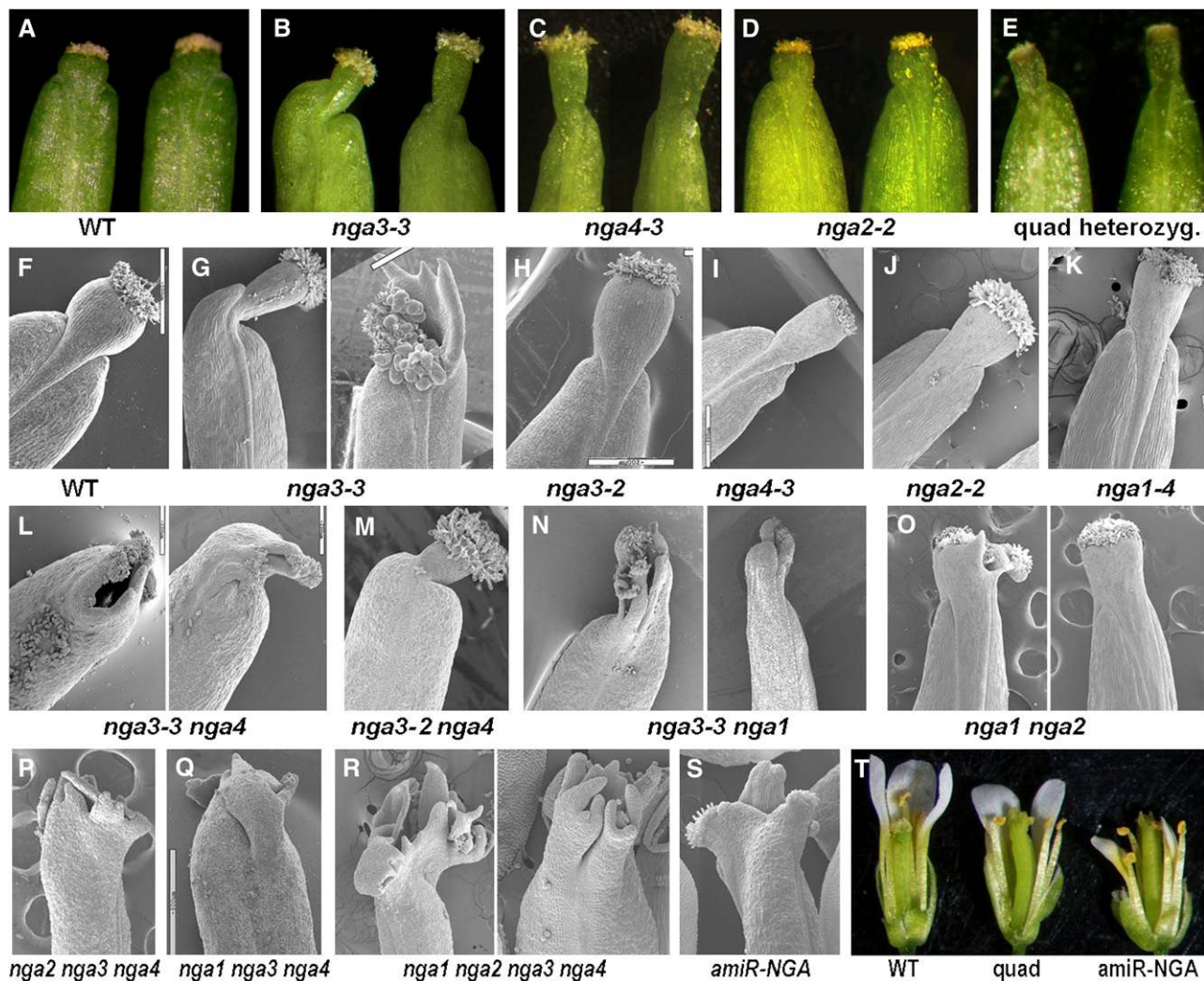


Figure 2. Phenotypes Caused by Different Mutations in the *NGA* Genes and Their Combinations.

(A) to (E) Apical regions of mature siliques from wild type (A), *nga3-3* (B), *nga4-3* (C), *nga2-2* (D), and a quadruple heterozygote *nga1-4/+ nga2-2/+ nga3-3/+ nga4-3/+* (E).

(F) to (S) Scanning electron micrographs of fruits 10 d after anthesis from the wild type (F), *nga3-3* (G), *nga3-2* (H), *nga4-3* (I), *nga2-2* (J), *nga1-4* (K), *nga3-3 nga4-3* (L), *nga3-2 nga4-3* (M), *nga3-3 nga1-4* (N), and *nga1-4 nga2-2* (O) and scanning electron micrographs of anthesis gynoecia from triple mutants *nga2-2 nga3-3 nga4-3* (P), *nga1-4 nga3-3 nga4-3* (Q), the quadruple mutant *nga1-4 nga2-2 nga3-3 nga4-3* (R), and from an amiR-*NGA* line carrying the amiRNA targeted against the four *NGA* genes (S).

(T) Flowers at approximately stage 14 of the wild type, *nga* quadruple mutants, and an amiR-*NGA* line. Note the protruding gynoecia and the abnormally short sepals and petals.

Since some of the alleles that we were using were not null, and to facilitate genetic analyses, we generated a line where an artificial miRNA targeting the four *NGA* genes was expressed under the control of the CaMV 35S promoter (amiR-*NGA* line; see Supplemental Figure 4A online) (Schwab et al., 2006). Four independent amiR-*NGA* lines showing identical phenotypes were selected, and RNA levels for the four *NGA* genes were shown to be significantly reduced (see Supplemental Figure 4B online). These lines showed a slightly stronger phenotype than the quadruple *nga1 nga2 nga3 nga4* mutant, probably due to the weak nature of the *nga1* allele used in our study. While carpel

development was similarly affected in the amiR-*NGA* lines and the quadruple mutant, all floral organs in amiR-*NGA* plants were shorter than in the *nga1 nga2 nga3 nga4* quadruple mutants (Figure 2T), and leaf serration and expansion was further enhanced (see Supplemental Figure 3B online), suggesting a general role for *NGA* genes in the regulation of lateral organ growth.

***NGA* Genes Are Widely Expressed throughout Development**

Real-time PCR analysis showed *NGA1*, *NGA2*, *NGA3/TOP1*, and *NGA4* genes to be expressed in all tissues tested (roots, stems,

leaves, and inflorescences; see Supplemental Figure 5A online), confirming the data available from the AtGenExpress expression atlas (Schmid et al., 2005). RNA in situ hybridization was performed on wild-type inflorescences. *NGA3/TOP1* and *NGA4* showed similar patterns of expression. *NGA3/TOP1* transcript was detected in the inflorescence and floral meristems, with stronger expression at the center of floral meristems at stages 2 and 3 (Figure 3A). Low *NGA3/TOP1* expression was found in developing floral organs with higher RNA levels at the distal portion of all growing primordia (Figure 3B). From stage 9 flowers, *NGA3/TOP1* RNA accumulated in the developing style and stigma and strongly in developing ovules (Figure 3C). *NGA4* RNA was detected in a similar pattern to *NGA3/TOP1* (Figures 3D and 3E).

NGA2 and *NGA1* patterns of expression were also similar to that described for *NGA3/TOP1* and *NGA4*, although some differences were apparent. In floral meristems, *NGA1* expression was detected preferentially in the adaxial half of the floral primordium (Figure 3I). *NGA1* expression was detected in all floral organ primordia with stronger expression levels in distal positions (Figures 3I and 3J). In the gynoecium primordium, up to stage 8, expression was strong at the apical end and in the adaxial (internal) side of the gynoeclial tube (Figure 3J). From stage 10, *NGA1* expression restricted to placental tissue, apical regions, and developing ovules, similar to what was observed for *NGA3/TOP1* and *NGA4* (Figures 3K and 3L). However, the expression levels at the apical end relative to expression in ovules appeared lower than those observed for *NGA3/TOP1* and *NGA4* at similar stages (cf. Figures 3C and 3E to 3L). *NGA2* expression pattern followed that of *NGA1* (Figures 3F to 3H).

To describe in more detail the spatial and temporal pattern of *NGA3/TOP1* expression, we generated transgenic lines harboring a *NGA3/TOP1* reporter construct, pMT5, in which a fragment of *NGA3/TOP1* upstream genomic sequence (−2728 to +12), including the first untranslated exon and the first and only intron, was fused to the β-glucuronidase (GUS) coding sequence.

Twelve out of 15 pMT5 independent lines showed identical patterns of GUS expression. In these lines, *NGA3_{PRO}*:GUS activity was found in a wide complex spatial pattern. In seedlings, GUS was detected in hypocotyls and cotyledons (Figure 3O), and strong signals were associated with very young leaf primordia, especially at the distal tip (Figure 3O; see Supplemental Figures 5B and 5C online). In expanded leaves, GUS was mainly detected in the hydathodes (see Supplemental Figure 5D online). In roots, signal was detected just above the root meristem and in lateral root primordia (Figures 3M and 3N). In reproductive structures, GUS activity matched RNA in situ hybridization results. In inflorescences, GUS activity was found at high levels in all meristems and young floral organ primordia (Figure 3Q). In developing flowers, GUS activity was associated with young floral organ primordia, with a maximum in the distal tips of the organs and decreasing as these organs grew and differentiated (Figure 3Q). In young carpel primordia (up to stages 7 to 8), GUS was detected at high levels in the apical end, decreasing toward the base (Figures 3Q and 3R). Previous to apical closure of the gynoecium (stage 9), GUS was detected only in the developing ovules and the apical ring of the gynoeclial tube (Figure 3R).

Expression in ovules was strongest in the nucellus (Figure 3S). From stage 10 to anthesis, expression in the apical gynoecium was maintained, but restricted progressively to the region between the style and the incipient stigma (Figures 3P and 3R). In ovules of anthesis or stage 14 flowers, GUS activity was uniformly detected (Figure 3T). After anthesis, GUS gradually disappeared from the apical end and was restricted to the abscission zone of floral organs and the embryo, where it was expressed uniformly through seed development (Figures 3P, 3U, and 3V). In summary, *NGA3_{PRO}*:GUS confirmed RNA in situ data through inflorescence and flower development and revealed the *NGA3/TOP1* expression pattern in vegetative tissues.

nga Mutants Are Affected in Auxin Responses

We had noted that the phenotype of *NGA*-overexpressing lines resembled plants with increased levels of auxin; for example, rosette morphology in 35S_{PRO}:*NGA3* plants is very similar to plants overexpressing the *YUC* auxin biosynthesis genes (Woodward et al., 2005; Kim et al., 2007). In addition, *NGA3_{PRO}*:GUS was detected in positions normally associated with high levels of auxin synthesis or accumulation, such as hydathodes, lateral root primordia, distal gynoecium, or ovule primordia (Aloni et al., 2003, 2006). To check whether *NGA* loss of function affected auxin responses, we determined classical auxin responses in *nga* mutants, such as root gravitropism, lateral root formation, and apical dominance. We found a modest reduction of all these traits in different *nga* mutant combinations (see Supplemental Figures 6B to 6D online).

It has been described that vascular development is induced by auxin (Reinhardt, 2003) and that the modification of auxin distribution, such as inhibiting auxin transport by treatment with naphthylphthalamic acid (NPA; a drug blocking polar auxin transport) affects vascular patterning in the gynoecium (Nemhauser et al., 2000). In the wild-type anthesis gynoecium, the medial veins running along the repla bifurcate near the valve-style junction to form ramified vascular fans (Figure 4A). We observed a slight reduction of these stylar fans in all *nga* single mutants, with a lower point of medial vein bifurcation (see Supplemental Figure 6A online). *nga3 nga4* double mutants showed an enhanced phenotype, with medial veins bifurcating at even lower positions and producing less stylar fans (Figure 4B). In a few severely affected flowers of *nga3 nga4* double mutants and in triple or quadruple mutants, vascular development was strongly perturbed: the medial vein did not bifurcate and stopped below the presumptive style, and in consequence no stylar fans were formed (Figure 4C). Conversely, 35S_{PRO}:*NGA3* gynoecia showed an extensive vascular development that resulted in increased stylar fans (Figure 4D). Lateral veins in all mutant backgrounds were less affected, being occasionally shorter than in the wild type (Figure 4).

Exogenous treatment with auxin, inhibition of auxin transport by NPA treatment, or genetically elevated auxin levels (in 35S_{PRO}:*YUC1* plants) did not alter *NGA3_{PRO}*:GUS expression, indicating that the *NGA3/TOP1* gene was not induced by high auxin levels (see Supplemental Figures 6E to 6I online). To determine if reducing auxin levels in the tissues in which *NGA3/TOP1* is normally expressed influences gynoecium development, we

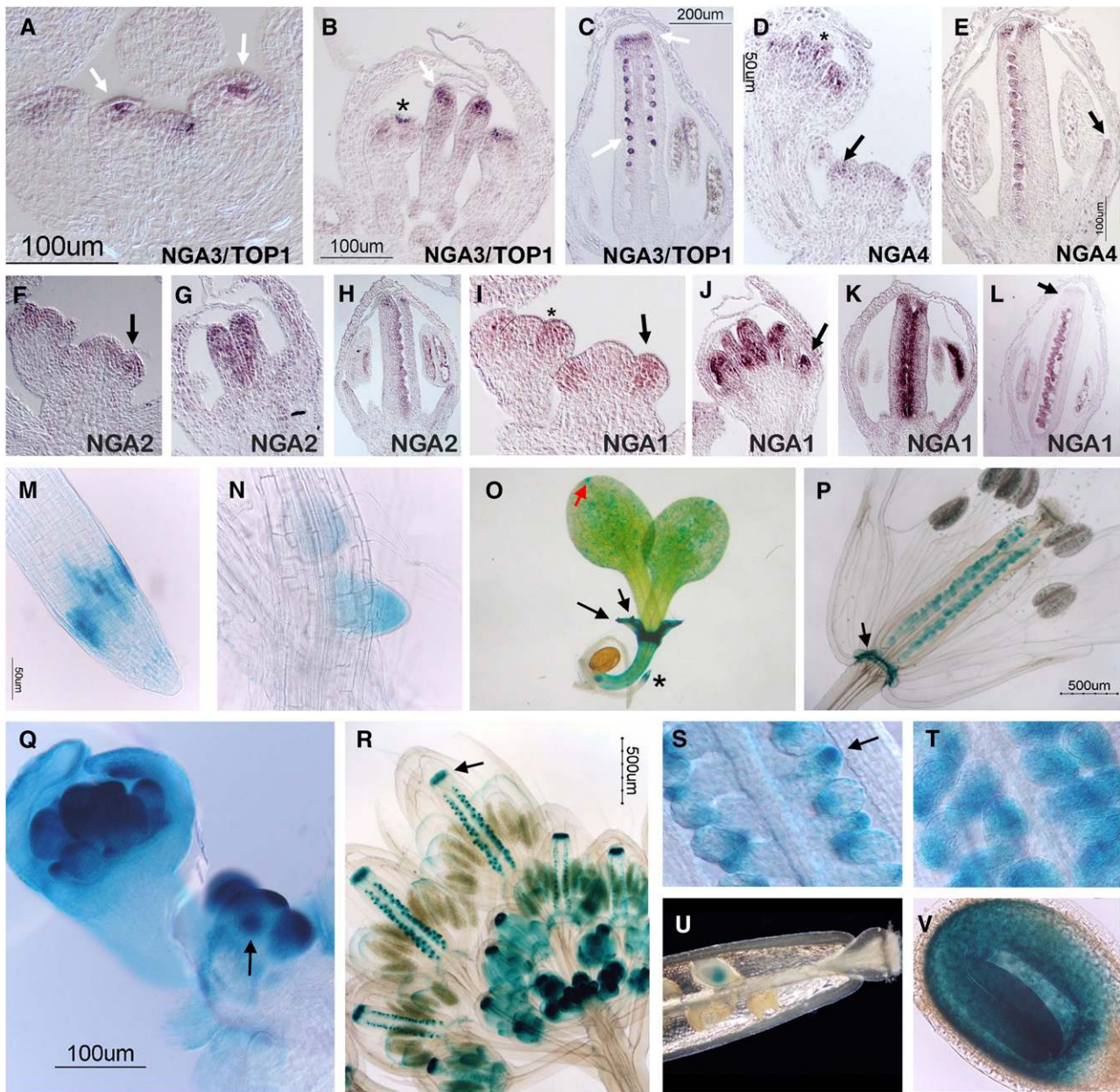


Figure 3. Expression Pattern of *NGA* Genes.

(A) to (L) RNA in situ hybridization in wild-type inflorescences and developing flowers.

(A) to (C) *NGA3/TOP1* RNA expression pattern.

(A) Inflorescence apex showing localized expression of *NGA3/TOP1* in the center of the floral meristems (arrows).

(B) Stage 8 flower showing strong *NGA3/TOP1* expression at the distal end of the gynoecial tube (arrow) and the tip of the stamens (asterisk).

(C) Stage 11 flowers showing *NGA3/TOP1* expression at the apical end of the gynoecium and the external surface of the ovules (arrows).

(D) and (E) *NGA4* RNA expression pattern.

(D) Inflorescence apex showing expression of *NGA4* in the floral meristems (arrow) and the apical portion of the growing gynoecium (asterisk) and the stamens of a stage 7 flower (top left).

(E) Stage 10 flower showing *NGA4* expression at the apical end of the gynoecium and the external surface of the ovules. *NGA4* expression is also detected in the tip of the growing petals (arrow).

(F) to (H) *NGA2* RNA expression pattern.

(F) Inflorescence apex. *NGA2* expression is detected in the adaxial half of the stage 2 floral primordium (arrow) and in the adaxial side of sepal primordia of the stage 4 flower on the left.

(G) Stage 7 flower. *NGA2* is detected in the adaxial side of the gynoecial tube.

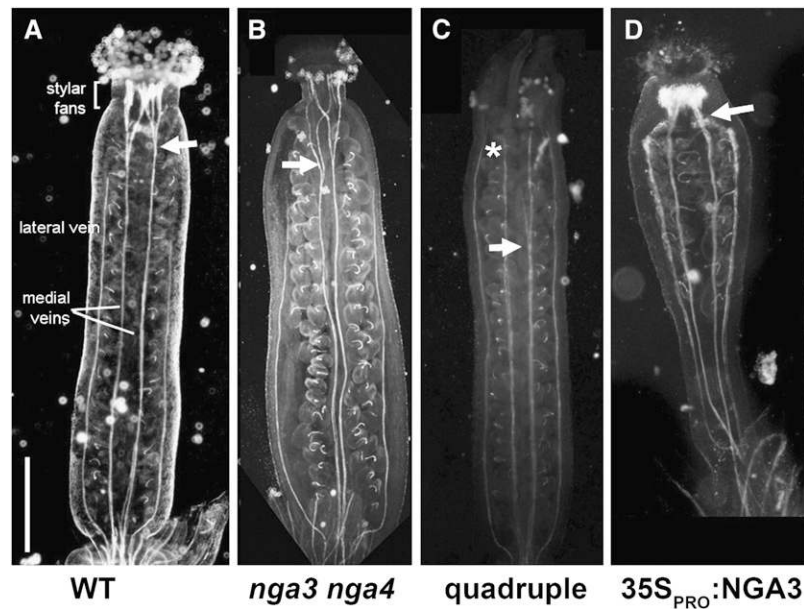


Figure 4. Vascular Patterning in Wild-Type, *nga* Mutant Combinations, and 35S_{PRO}:NGA3 Gynoecia at Anthesis.

(A) The wild type.

(B) *nga3-3 nga4-3* double mutants. Vascular fans in the style appear very reduced.

(C) *nga1-4 nga2-2 nga3-3 nga4-3* quadruple mutant. Medial vein bifurcation is found at a low position (arrow) or is absent (asterisk). No vascular fans are formed.

(D) 35S_{PRO}:NGA3. Vascular fans at the style overproliferate. Bifurcation of the medial vein is distalized.

Bar = 500 μ m. Arrows indicate medial vein primary bifurcation.

expressed the *laaL* gene from the *NGA3/TOP1* promoter (NGA3_{PRO}:*laaL*). *laaL* is a bacterial gene that encodes an enzyme that inactivates free auxin through conjugation to Lys (Jensen et al., 1998). We found that in NGA3_{PRO}:*laaL* transgenic plants, >50% of the gynoecia had reduced apical tissues, similar to that

observed in *nga* double mutant combinations (Figure 5). These data are consistent with the idea that *NGA3/TOP1* could be promoting auxin accumulation in the apical gynoecium and that the *nga* phenotypes were related to reduced auxin levels in this domain.

Figure 3. (continued).

(H) Stage 9 flower showing *NGA2* expression at the apical end of the gynoecium and the placental tissue. *NGA2* expression is also detected in the tip of the growing petals.

(I) to (L) *NGA1* RNA expression pattern.

(I) Inflorescence apex. *NGA1* expression is similar to *NGA2* in (F). *NGA1* is expressed in the adaxial side of the stage 2 flower (arrow) and the adaxial side of sepal primordia in the stage 4 flower on the left (asterisk).

(J) Stage 7 flower. *NGA1* is detected in the adaxial side of the gynoecial tube, the stamen primordial, and in the tip of the petal primordia (arrow).

(K) Stage 9 flower showing *NGA1* expression in the placenta and the apical end of the developing gynoecium.

(L) Stage 11 flower similar to that shown in (C). Expression of *NGA1* is detected in the ovules but is very reduced in apical positions (arrow).

(M) to (V) NGA3_{PRO}:GUS histochemical staining.

(M) Primary root of a 5-d-old seedling.

(N) Emerging lateral root primordium.

(O) Young seedling showing expression in the emerging leaves (black arrow), the distal end of the cotyledons (red arrow), and the root tip (asterisk).

(P) Stage 14 flower (after anthesis). GUS activity is detected in the ovules, the abscission zone of floral organs (arrow), and in a thin layer between the style and the stigma.

(Q) Inflorescence apex. GUS activity is detected in the center of emerging floral primordia (arrow) and the tip of floral organs (stage 7 flower on the left).

(R) GUS staining in an inflorescence with flowers of different stages. Staining in developing flowers is mainly associated with the apical end of gynoecia (arrow), the ovules, and the distal portions of developing petals and stamens.

(S) Ovule primordia of a stage 12 flower. GUS activity is detected mainly in the outer integument and the nucellus (arrow).

(T) Stage 14 flower showing uniform GUS activity in the ovules.

(U) In stage 17 fruits, GUS detection is restricted to the developing embryo.

(V) Mature seed showing uniform GUS staining in the embryo.

NGA and STY Genes Cooperatively Interact to Activate YUC4 and to Direct Style Development

The *STY1* gene encodes a RING-finger transcription factor belonging to a small family of nine members (SHI-like). *sty1* mutants show subtle defects in style and stigma development (Figures 6A, 6C, 6E, and 6G), which increase in severity when combined with mutations in the other members of the family, similarly to what we observed for *nga* multiple mutants (Kuusk et al., 2006). Moreover, the overexpression of *STY1* shows similarities to that of *NGA3/TOP1*, such as the narrow shape of leaves or the massive vascular fans in the style (Kuusk et al., 2002). In addition, the *STY1* and *NGA3/TOP1* patterns of expression are almost identical (Kuusk et al., 2002).

The combination of *nga3/top1* and *sty1* mutations severely altered gynoecium development. *nga3-3 sty1-1* carpels appeared unfused at the apical end and lacked most of the style and the stigma, which were transformed into leafy protrusions and frequently developed horn-like structures (Figures 6B and 6F). *nga3 sty1* mutants had reduced fertility, probably as a consequence of the reduction of the transmitting tissues and subsequent lack of ovule fertilization. *nga3 sty1* double mutants resembled multiple combinations of mutations in the SHI-like gene family (Kuusk et al., 2006) or in the NGA family (Figure 2R). Moreover, in a *nga3 sty1 sty2* triple mutant, the *sty2* mutation did not further enhance the *nga3 sty1* phenotype (Figures 6D and 6H) and, conversely, neither did *nga4* in a triple *nga3 nga4 sty1* mutant (see Supplemental Figure 7 online). We introduced a *STY1_{PRO}:GUS* reporter gene (Kuusk et al., 2002) into a *nga3 nga4* mutant background and into an amiR-NGA line. In both backgrounds, we found *STY1* pattern of expression to be similar to the wild type, indicating that *STY1* was not regulated by NGA activities (Figures 6K and 6L). Likewise, *NGA3_{PRO}:GUS* activity was unaffected in a *sty1 sty2* background (Figures 6I and 6J). Taking these data together, it appears that the NGA and SHI-like factors do not regulate each other's expression, but probably SHI-like and NGA proteins require each other to exert their functions, at least in the gynoecium context.

Interestingly, a gene driving auxin synthesis, *YUC4*, has been suggested as a putative direct *STY1* target (Sohlberg et al., 2006). *YUC4* is expressed in wild-type gynoecia in the apical

domain and in the developing ovules, overlapping with both *STY1* and *NGA3/TOP1* expression domains. Since *nga* mutant phenotypes mimicked the effect of reducing auxin levels in the apical gynoecium, we wondered whether *YUC4* activation could be dependent on NGA activity. To test this hypothesis, a *YUC4_{PRO}:GUS* reporter line (Cheng et al., 2006) was crossed to an amiR-NGA line, which as shown in Figures 7A and 7B, still expresses *STY1* in the apical gynoecium. *YUC4* expression was very reduced or absent in apical gynoecial tissues of this line, indicating that STY factors may require NGA activity to upregulate the *YUC4* gene in the style (Figures 7C and 7D). Since *YUC2*, an additional member of the *Arabidopsis* YUC family, is also expressed in the style, we also checked *YUC2_{PRO}:GUS* expression (Cheng et al., 2006) in amiR-NGA lines. As for *YUC4*, *YUC2* expression was absent or very reduced in amiR-NGA apical gynoecia (Figures 7E and 7F).

No positive interactions were found between *NGA3/TOP1* and *STY1* in a yeast two-hybrid assay or in a bimolecular fluorescence complementation experiment in planta (data not shown). Still, this did not exclude the possible synergy of both factors on putative common targets to direct apical gynoecium development. To test for this interaction, we generated a *35S_{PRO}:STY1 35S_{PRO}:NGA3* line. We found a new phenotype in the double overexpressors, dramatically different from that of the individual *STY1* and *NGA3/TOP1* overexpressing lines. As previously described, *NGA3/TOP1* overexpression strongly affected gynoecium patterning, which developed fruits with long gynophores, reduced ovaries, and enlarged misshaped repla (Figure 8B). Vegetative phenotypes included narrow leaves, altered phyllotaxis, and smaller plant size (Figure 1). The *35S_{PRO}:STY1* phenotypes consisted of ectopic style tissue in patches in the center of the valves, which caused wrinkled ovaries to develop, and similar but weaker vegetative phenotypes to *35S_{PRO}:NGA3* plants (Figure 8A; Kuusk et al., 2002). In *35S_{PRO}:NGA3 35S_{PRO}:STY1* lines, overall plant size was further reduced. Leaf size, internode length, and flower size were strongly decreased (Figure 8G). Surprisingly, in the floral context, overall gynoecium morphology was much less affected than in the individual overexpressing lines. The relative proportions of gynophore, ovary, and apical tissues were restored to the wild type, although overall fruit size was strongly reduced (Figure 8C). While a clear distinction of valve, valve margin, and replum was observed, most epidermal cells in the valves showed the characteristic morphology of style cells, with regular morphology, early differentiating stomata, and typical crenellations (Figures 8D to 8F, 8H, and 8I). The replacement of valve tissues by style cells in the ovary of *35S_{PRO}:NGA3 35S_{PRO}:STY1* plants strongly supports the hypothesis that the STY and NGA proteins act cooperatively to direct style identity specification.

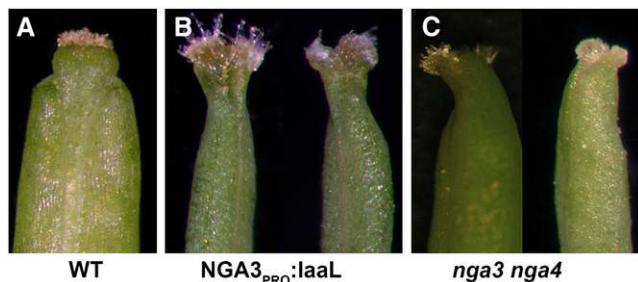


Figure 5. Effect in the Fruits of Reducing Auxin Levels in the *NGA3/TOP1* Expression Domain.

Apical regions of young fruits of the wild type (A), *NGA3_{PRO}:laaL* (B), and *nga3-3 nga4-3* double mutants (C). Styles of *NGA3_{PRO}:laaL* and *nga3 nga4* fruits appear poorly developed and partly unfused.

DISCUSSION

The NGA Genes Act Redundantly to Direct Fruit Patterning in the *Arabidopsis* Gynoecium in a Dose-Dependent Manner

We have shown here that the NGA factors are redundantly required for style and stigma specification and that this

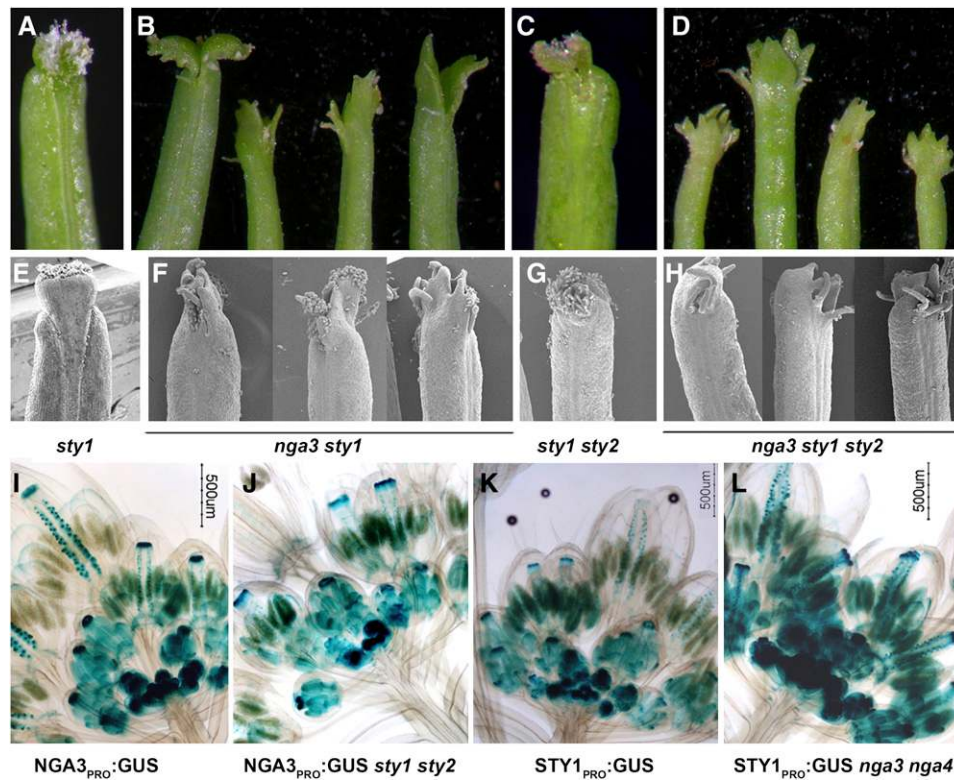


Figure 6. Genetic Interactions between *NGA* and *STY* Family Members.

Apical regions of mature siliques ([A] to [D]) and scanning electron micrographs of anthesis gynoecia ([E] to [H]).

(A) and (E) *sty1* mutant.

(B) and (F) *nga3-3 sty1* double mutants. The phenotype is similar to the quadruple *nga* mutant in Figure 2.

(C) and (G) *sty1 sty2* double mutant. The phenotype of the unfused style is enhanced with respect to the *sty1* single mutant in (A).

(D) and (H) *nga3-3 sty1 sty2*. The phenotype is identical to the double *nga3-3 sty* mutants.

(I) and (J) Histochemical detection of *NGA3_{PRO}::GUS* in wild-type (I) or *sty1 sty2* double mutant inflorescences (J). No significant differences were found.

(K) and (L) Histochemical detection of *STY1_{PRO}::GUS* in wild-type (K) or *nga3 nga4* double mutant inflorescences (L). Likewise, *STY1* expression is not significantly altered in the *nga3 nga4* mutant background.

redundancy is dosage dependent. While single mutants in the different *NGA* loci show subtle or no defects in carpel morphology, higher-order mutant combinations exhibit increasingly enhanced defects in apical gynoecium development, which is completely disrupted in the quadruple mutant. Among all the alleles used in this study, only *nga3-1* and *nga4-3* are likely to be null, both of them showing a weak phenotype in the style. *nga1-4* and *nga2-2* do not exhibit abnormal gynoecium development, but since they are probably not null, it is not possible to conclude whether their functions are completely redundant or not. The strongest phenotype corresponds to the *nga3-3* allele, where the *NGA3* gene bears an Spm fragment insertion toward the end of the B3 domain, which might produce a truncated protein that could have an antimorphic effect. The style phenotype of the quadruple mutant had already been preliminary described when the *NGA* genes were targeted by an amiRNA as proof of concept for the use of amiRNAs in functional studies (Alvarez et al., 2006).

The four members of the *NGA* family share a common organization, with a single N-terminal B3 DNA binding domain and three short conserved motifs in the C-terminal half (see Supple-

mental Figures 1B and 8A online). Sequence similarity is high throughout the B3 domain, but also extends to the rest of the protein, being higher between the pairs *NGA1/NGA2* and *NGA3/NGA4*. Conservation of protein sequence fits well with the highly similar phenotypes of plants overexpressing any of the four *NGA* genes. In addition, expression patterns of *NGA* genes are also similar. The four *NGA* loci are located toward the telomeric regions of different chromosomes, in regions that have been shown to correspond to duplicated blocks (Blanc et al., 2003). A cumulative benefit related to gene dosage effects and/or benefits derived from buffering against dominant-negative mutations can explain the frequency of functional redundancy. Regulatory proteins are often part of multimeric complexes particularly sensitive to gene dosage and dominant-negative mutations; accordingly, transcription factors are overrepresented among the duplicated genes retained in the *Arabidopsis* genome (Blanc and Wolfe, 2004). The unusual level of redundancy found in the *NGA* genes is in agreement with their proposed regulatory role directing carpel development and parallels that of *STY* family members in highly related functions, suggesting a concerted

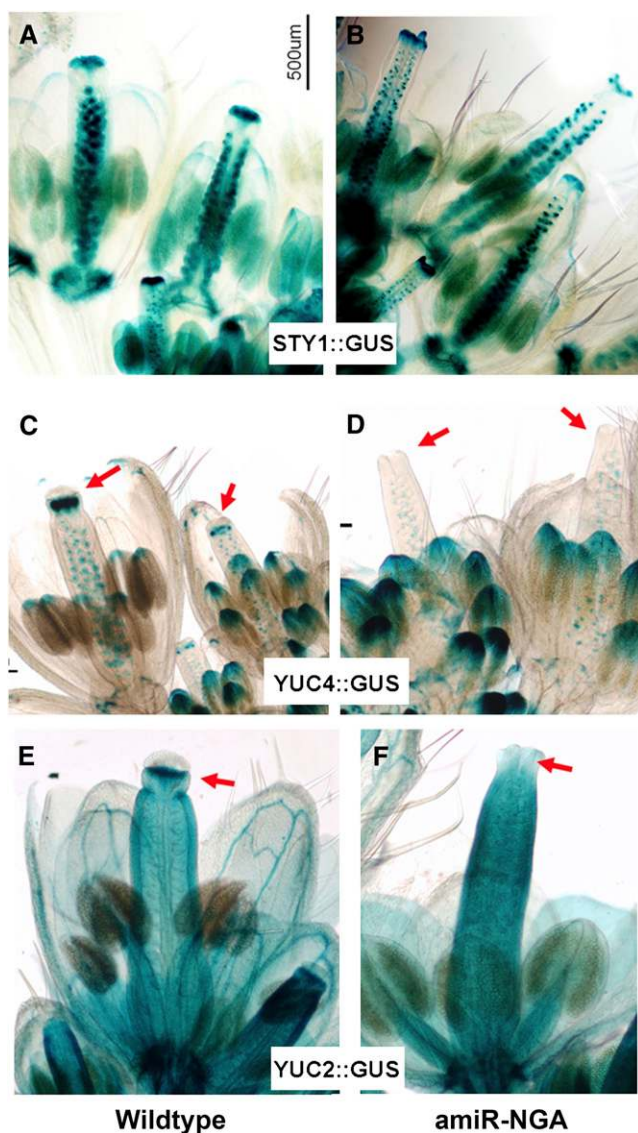


Figure 7. Reduced NGA Activity Severely Affects *YUC2* and *YUC4* Expression in the Style.

Histochemical detection of GUS activity driven by *STY1* ([A] and [B]), *YUC4* ([C] and [D]), or *YUC2* promoters ([E] and [F]) in inflorescences of the wild type ([A], [C], and [E]) and an amiR-NGA line ([B], [D], and [F]). While *STY1* expression is not affected by the reduced NGA activity in the amiR-NGA lines, *YUC4* and *YUC2* are activated only in the style of wild-type gynoecia and not in the amiR-NGA lines. Arrows indicate styles of flowers at different stages of development.

action of NGA and STY factors that could require an adequate stoichiometry of both activities (see below).

Database mining has not revealed any NGA homologs with a similar domain organization outside the angiosperms. Intriguingly, while the copy number of NGA genes in *Arabidopsis* is consistent with a single ancestor previous to monocot/dicot divergence, in species where whole-genome sequence is available, NGA homologs with similar domain organization are found

frequently in several copies that could possibly be derived from independent duplication events (for example, at least five related proteins are found in *Oryza sativa*, two in *Populus trichocarpa*, and two in *Vitis vinifera*; see Supplemental Figure 8 and Supplemental Data Set 1 online for alignments and a phylogenetic tree). This suggests that maintaining multiple copies of NGA genes could be beneficial for reproductive success, although deeper phylogenetic and functional analyses are required to support this hypothesis.

NGA Proteins Are Involved in Auxin Signaling Pathways

Both gain- and loss-of-function mutations in NGA genes cause phenotypes related to altered auxin homeostasis or signaling pathways. For example, several classic auxin responses, such as apical dominance or gravitropism, are moderately altered in the multiple combinations of nga mutants, like in plants with reduced auxin levels or impaired auxin sensing (Timpote et al., 1995; Hobbie et al., 2000; Cheng et al., 2007). Likewise, vascular development in the gynoecia of nga mutants is reduced (Cheng et al., 2006). In addition, the severe epinasty of rosette leaves in 35S_{PRO}:NGA3 lines is similar to that caused by increased auxin production, as in lines overexpressing *YUC* or the bacterial *laaM* gene (Romano et al., 1995; Zhao et al., 2001; Marsch-Martinez et al., 2002). These phenotypes suggest that nga mutants could have reduced levels of auxin. Consistent with this idea, we have shown that a reduction of auxin levels in the NGA3/*TOP1* expression domain (as in NGA3_{PRO}:*laaL* lines) mimics some of the nga loss-of-function phenotypes.

Auxin accumulation in the apical gynoecium is likely a consequence of direct auxin synthesis in this domain (Aloni et al., 2006), and here we show that lack of NGA activity leads to a failure to activate *YUC2* and *YUC4* in these positions. Our data are thus consistent with a role of NGA genes in driving auxin synthesis in the apical gynoecium through the upregulation of *YUC* gene expression. However, outside of the apical gynoecium, NGA proteins appear not to be required to activate *YUC2* and *YUC4* transcription. While absent in the style of amiR-NGA lines, *YUC2* and *YUC4* expression is normal in the rest of the flower, suggesting that independent activation of *YUC* genes by other factors takes place in these other domains. Alternatively, the residual NGA activity in the amiR-NGA lines may still activate *YUC* expression in these nonapical gynoecium positions. *YUC4* is not constitutively expressed in the 35S_{PRO}:NGA3 line (see Supplemental Figure 9 online), so it is likely that additional gene functions are required along with NGA activity for *YUC2* and *YUC4* upregulation, suggesting a complex scenario for spatial and temporal regulation of the *YUC* genes.

Many different studies support the auxin gradient hypothesis for gynoecium patterning at the apical-basal axis (reviewed in Balanza et al., 2006). The requirement for locally high auxin levels at distal positions of the gynoecial tube has been suggested by experiments showing that localized application of exogenous auxin at the apical end of developing gynoecia is able to restore carpel closure and style and stigma development in *sty1 sty2* mutants (Staldal et al., 2008). Likewise, treatment with NPA, an inhibitor of polar auxin transport that would cause pooling of auxin in the apical domain, restores style development in several

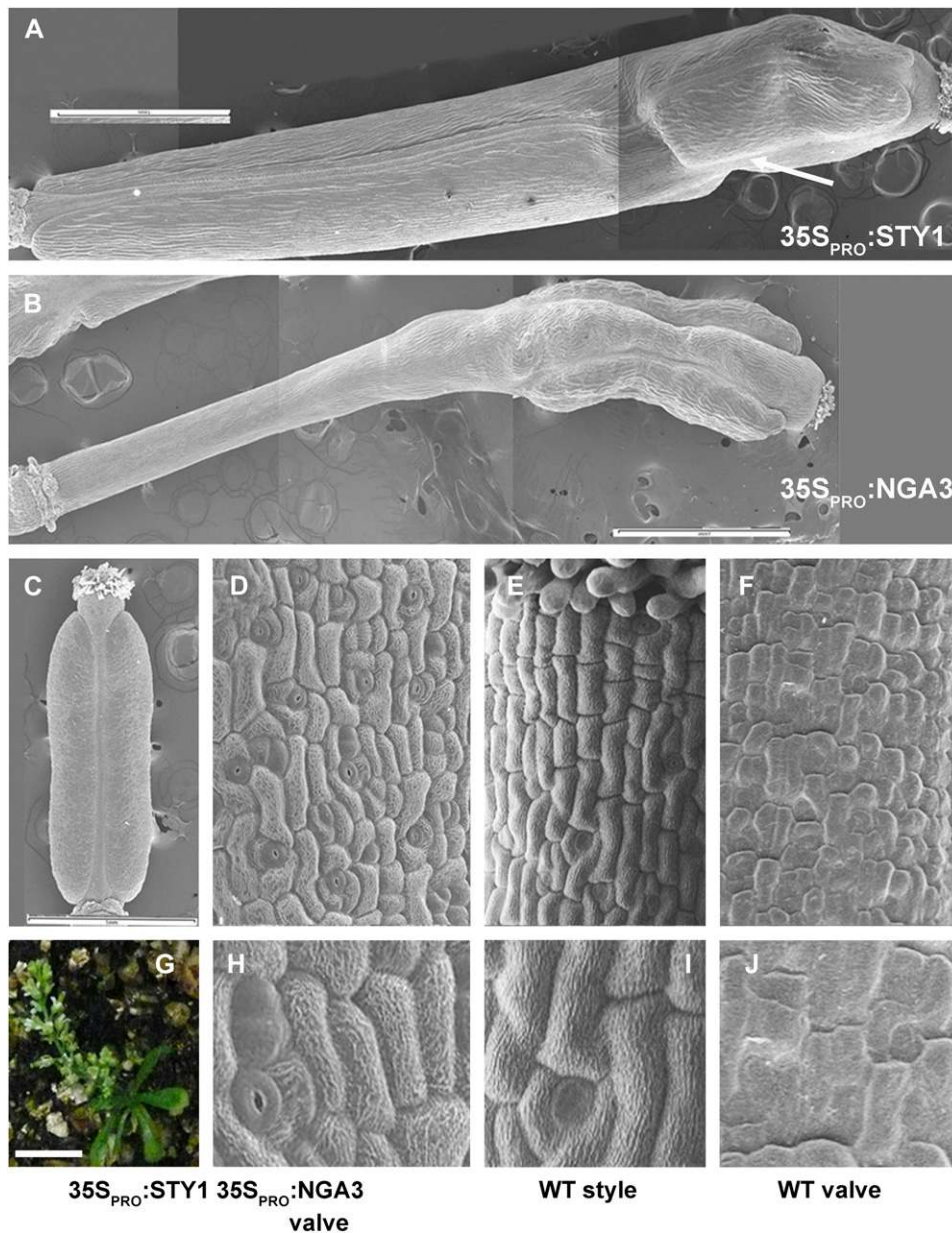


Figure 8. Phenotypic Effects of the Ectopic Expression of *NGA3/TOP1*, *STY1*, or Both in Fruit Morphology.

(A) to (F) and (H) to (J) Scanning electron micrographs. Bars = 50 μm in (D) to (F) and 10 μm in (H) to (J).

(A) Mature $35S_{\text{PRO}}::\text{STY1}$ silique. Stripes of ectopic style tissue in the center of the apical half of the valves cause the fruits to wrinkle (arrow).

(B) Mature $35S_{\text{PRO}}::\text{NGA3}$ silique. The gynophore is elongated, the valves are dramatically reduced, and the replum appears wide and with an abnormal cell orientation.

(C) Mature $35S_{\text{PRO}}::\text{NGA3}$ $35S_{\text{PRO}}::\text{STY1}$ silique. Fruit morphology is restored to wild-type-like appearance, with normal relative proportions of gynophore, valve, replum, and style. However, overall fruit size is dramatically decreased. Note that the same magnification applies for (A) to (C) (bars = 1 mm). Valves are covered by cells with typical style morphology.

(D) and (H) Close-up view of epidermal cells in the central region of the valves of $35S_{\text{PRO}}::\text{NGA3}$ $35S_{\text{PRO}}::\text{STY1}$ gynoecium at anthesis. Cells show typical column-like morphology, and crenellations of style cells and early differentiating stomata are also visible.

(E) and (I) Close-up view of the style of a wild-type gynoecium.

(F) and (J) Close-up view of the epidermal cells of a wild-type valve.

(G) Dramatically reduced plant size and internode elongation of a $35S_{\text{PRO}}::\text{NGA3}$ $35S_{\text{PRO}}::\text{STY1}$ plant. Bar = 1 cm.

[See online article for color version of this figure.]

unrelated mutants with defects in apical gynoecium development (Nemhauser et al., 2000; Staldal et al., 2008). In this work, we show that reducing auxin levels in the *NGA3/TOP1* expression domain causes poor development of the style and the stigma, thus providing direct support for the requirement of auxin for correct specification of apical gynoecium development.

NGA, STY, and Style Specification

Striking similarities are found between the *NGA* and the *STY* gene families. While the corresponding gene products are unrelated, loss-of-function phenotypes for multiple mutants in *NGA* genes or in *STY* genes are very similar. Both families also share a high level of functional redundancy among their members and show dosage-dependent loss-of-function phenotypes. Moreover, expression patterns of *NGA* and *STY* genes are similar, and, in fact, *NGA3/TOP1* and *STY1* have almost identical patterns of expression. Our expression analyses indicate that *STY1* and *NGA3/TOP1* do not regulate each other at the transcriptional level. Moreover, significant homology is found among fragments of *NGA3/TOP1* and *STY1* upstream genomic regions, suggesting that they might be coregulated. Taken together, these data suggest that *NGA* and *STY* could act at the same level to regulate putative common targets. The strong phenotypes of *nga3 sty1* double mutants suggest that *NGA* and *STY* proteins could be required to cooperatively direct style formation. Additional support for this idea is provided by the striking phenotype of 35S_{PRO}:*NGA3* 35S_{PRO}:*STY1* plants, where valve cells are replaced by style cells. While it is possible that the *NGA* and *STY* proteins physically interact, we have thus far not been able to detect such interaction. A possible scenario is that additional factors are required in this putative style-promoting complex. This hypothesis is in accordance with the phenotype of 35S_{PRO}:*NGA3* 35S_{PRO}:*STY1*, which promotes ectopic style development only in the valves, suggesting that factors specifically present in this domain could contribute to *NGA*-*STY* activity. Different pieces of evidence suggest *CRC*, a member of the *YABBY* family expressed in valve tissues, as a candidate factor for this predicted interaction (Bowman and Smyth, 1999). Thus, *crc* mutants show defects in gynoecium closure and a reduction of style and stigma (Alvarez and Smyth, 1999).

The Distribution of Tissues in the Gynoecium

The phenotype of loss-of-function mutations in the *NGA* genes indicates a role for *NGA* factors in directing style and stigma development; in fact, the effect of overexpressing simultaneously *STY1* and *NGA3/TOP1* supports this idea. However, the phenotypes of *NGA* gain-of-function lines are also compatible with a possible role of *NGA* factors regulating the distribution of tissues within the gynoecium. In general, 35S_{PRO}:*NGA3* lines show an altered patterning of the different regions of the carpel, most frequently a reduction of the ovary at the expense of an enlarged gynophore and style, but also an expansion of the replum and the valve margin region into the reduced valves. Thus, patterning along both apical-basal and medial-lateral axes is compromised. The apical-basal defects in 35S_{PRO}:*NGA3* lines are reminiscent of the phenotype of the 35S_{PRO}:*HEC1* or 35S_{PRO}:*HEC3* lines (Gremski et al., 2007), while the medial-lateral phe-

notypes resemble that caused by overexpression of *INDEHISCENT* (*IND*), a key factor for the development of the dehiscence zone in the valve margins and the closest homolog to the *HEC* genes (Liljegren et al., 2004). While the molecular bases for the parallelisms of the observed phenotypes are still unclear, it would be interesting to test if they depend on genetic or physical interactions between the *NGA* and the *HEC/IND* factors.

The striking effect of constitutive coexpression of *STY1* and *NGA3/TOP1* factors also awaits further studies. One possible explanation for the observed effects could be as follows: when high levels of *STY1* are available, as in the apical domain of the gynoecium or in the 35S_{PRO}:*STY1* lines, *NGA3/TOP1* acts cooperatively with *STY1* to direct style formation; however, when *STY1* factors are not available, overexpression of *NGA3/TOP1*, through still unknown mechanisms, interferes with genetic pathways directing tissue distribution in the gynoecium.

In summary, we have characterized a small subfamily of highly redundant B3 transcription factors, the *NGA* family, with a key role in style specification. Together with previous work, our data point to a complex landscape of regulatory activities and hormonal pathways established in the developing gynoecium that will need to be addressed in the future.

METHODS

Plant Material and Growth Conditions

Arabidopsis thaliana plants were grown in cabinets at 21°C under long-day (16 h light) conditions, illuminated by cool-white fluorescent lamps (150 $\mu\text{E m}^{-2} \text{s}^{-1}$), in a 1:1:1 mixture of sphagnum:perlite:vermiculite.

The *Arabidopsis* plants used in this work were from the Col ecotype. The *top1-1D* line was identified in an activation tagging mutagenized population (Weigel et al., 2000). *nga3-2*, *nga3-3*, *nga4-2*, and *nga4-3* were identified screening the AMAZE collection. *nga3-3* has a fragment of a *En-1* element inserted at position 404; *nga3-2*, *nga4-2*, and *nga4-3* carry *En-1* elements at positions 861, -25, and 125, respectively. *nga3-1*, *nga1-4*, and *nga2-2* mutants were obtained from the ABRC Stock Center. *nga3-1* has a T-DNA inserted at position 221 (line Sail_232_E10). *nga1-4* bears a T-DNA insertion 171 bp downstream the STOP codon (line WiscDsLox429G06), while *nga2-2* carries an *En-1* insertion at position 572 (line SM.20993). *sty1 sty2* mutant seeds and the *STY1*_{PRO}:*GUS* and 35S_{PRO}:*STY1* lines were kindly donated by Eva Sundberg (Kuusk et al., 2002). 35S_{PRO}:*YUC1*, *YUC2*_{PRO}:*GUS*, and *YUC4*_{PRO}:*GUS* were kindly provided by Yunde Zhao (Cheng et al., 2006).

The 35S_{PRO}:*NGA* constructs were generated by PCR amplification of the different *NGA* ORFs to introduce *Sall* and *Bam*HI flanking restriction sites, except for *NGA4*, where the *Xho*I site was preferred to *Sall*, and subsequently cloned into *Sall*-*Bam*HI-digested pBIN-JIT vector (Ferrández et al., 2000). The 35S_{PRO}:*NGA3* (PMT17) construct was generated by cloning the *NGA3* ORF into *Bam*HI and *Eco*RI site of the pGreenII0229-35S vector (www.pgreen.ac.uk). amiR-*NGA* lines were generated as previously described (Schwab et al., 2006). The sequence of the mature miRNA targeting all four *NGA* genes was 5'-UACUU-UGUCGAACAUGUGCCC-3'. The corresponding amiRNA was PCR amplified (see Supplemental Table 1 online for primer sequence) according to the protocol provided via WMD2 Web MicroRNA Designer (<http://wmd2.weigelworld.org>) with the greatly appreciated help of Rebecca Schwab and cloned into *Sall*-*Bam*HI sites of the pBIN-JIT vector. Transgenic plants were selected based on the kanamycin resistance.

The *NGA3*_{PRO}:*laaL* construct was generated by replacing the *GUS* coding sequence with the coding sequence of the *laaL* gene from

Pseudomonas syringae into a *Bam*HI-*Sac*I-digested pMT5 plasmid (see below). Transgenic plants were selected based on kanamycin resistance.

Cloning of *top1-1D* and Isolation of Loss-of-Function Alleles

Plasmid rescue on the original *top1-1D* line was performed as described by Weigel et al. (2000).

To identify insertion alleles of *nga3/top1* and *nga4*, we screened a population of *Arabidopsis* Col plants that carries ~50,000 independent insertions of the autonomous maize transposable element *En-1* using previously established methods (Baumann et al., 1998). Primers used in PCR reactions were SS020 and SS023. Each oligo was used with both *En-1*-specific primers En205 and En8130. Genomic DNA from single plants was used to PCR amplify the region of *En-1* insertion, and subsequent sequence analyses identified the insertion site.

Homozygous plants with single Spm or T-DNA insertions were identified in the progeny of backcrosses of each mutant allele to wild-type Col by genomic DNA gel blot analyses probed with the full ORF of the corresponding NGA gene following standard procedures.

Phenotypic Characterization

For scanning electron microscopy, samples were vacuum infiltrated with 4% formaldehyde (w/v) in 1 × PBS for 10 min and fixed with fresh solution for 16 h at 4°C. Samples were dehydrated in an ethanol series and critical point dried in liquid CO₂ (Polaron E300 apparatus). Dried samples were mounted on stubs; when necessary, several outer whorl organs of individual flowers were removed manually. Then, samples were coated with gold palladium (4:1) in a Sputter Coater SCD005 (BALTEC). Scanning electron microscopy was performed with a JEOL JSM-5410 microscope (10 kV).

Vascular Clearing

Anthesis gynoecia from wild-type and mutant lines were fixed, cleared in chloralhydrate, and mounted according to Weigel and Glazebrook (2002) to be viewed under dark-field microscopy.

Auxin Responses

Seeds were grown on vertical plates. For lateral root counts, roots were counted at 10 d after planting. For root reorientation assays, plates were rotated 90° with respect to gravity and photos were taken 24 h later. Root angles were calculated in Adobe Photoshop using the measure tool.

Apical dominance was measured by quantifying the number of lateral inflorescences longer than 1 cm from the rosette from 15 plants per genotype when the main inflorescence reached 10 cm.

Expression Analyses

For quantitative PCR, 100 ng of total RNA was used for cDNA synthesis performed with the iScript™ cDNA synthesis kit (Bio-Rad), and the qPCR master mix was prepared using the iQTM SYBR Green Supermix (Bio-Rad). Primers used to amplify the NGA genes were as follows: OMNG48 and OMNG49 for *NGA1*, OMNG46 and OMNG47 for *NGA2*, OMNG42 and OMNG43 for *NGA3*, and OMNG44 and OMNG45 for *NGA4*. Results were normalized to the expression of the *UBIQUITIN-CONJUGATING ENZYME21* (*UBC21*) mRNA, amplified with UBC21F and UBC21R primers. PCR reactions were run and analyzed using the ABI PRISM 7700 sequence detection system.

RNA in situ hybridization with digoxigenin-labeled probes was performed on 8-μm longitudinal paraffin sections of Col inflorescences as described by Ferrándiz et al. (2000). *NGA3/TOP1* RNA antisense and

sense probes were generated from a 423-bp fragment of the *NGA3/TOP1* cDNA (positions 655 to 1077), *NGA4* from a 320-bp fragment (positions 655 to 987), *NGA2* from a 388-bp fragment (positions 513 to 900), and *NGA1* from a 372-bp fragment (positions 505 to 877). All fragments were cloned into the PCRII vector (Invitrogen), and sense and antisense probes were synthesized using the corresponding SP6 or T7 polymerases.

The pMT5 construct (*NGA3_{PRO}*-GUS) was generated by cloning a fragment of *NGA3/TOP1* upstream genomic sequence (−2728 to +12) PCR amplified from Col genomic DNA into *Hind*III-*Bam*HI sites of a pGREENII0029 vector (<http://www.pgreen.ac.uk>) previously modified by introducing the GUS coding sequence from pBI101.2.

For GUS histochemical detection, samples were treated for 15 min in 90% ice-cold acetone and then washed for 5 min with washing buffer (25 mM sodium phosphate, 5 mM ferrocyanide, 5 mM ferricyanide, and 1% Triton X-100) and incubated from 4 to 16 h at 37°C with staining buffer (washing buffer + 1 mM X-Gluc). Following staining, plant material was fixed, cleared in chloralhydrate, and mounted according to Weigel and Glazebrook (2002) to be viewed under bright-field microscopy. All detections were made in heterozygous lines for the reporter transgene.

Genetic Combinations

Homozygous single mutants were cross-fertilized, and double mutants were identified among the F2 segregants by novel phenotypes and confirmed by genotyping or by segregation of F3 progenies.

For genotyping *nga1-4*, PCR with primers OTL2RWT and p745 gave a 0.6-kb product for the mutant allele and PCR with primers OTL2RWT and SS071 produced a 1-kb fragment for the wild-type allele. For genotyping *nga2-2*, PCR with primers OMNG14 and En8130 gave a 0.6-kb product for the mutant allele and PCR with primers OMNG14 and OMNG15 produced a 0.7-kb fragment for the wild-type allele. For genotyping *nga3-3*, PCR with primers SS044 and SS043 produced a 1.5-kb fragment for the wild-type allele and 2.1 kb for the *nga3-3* allele. For genotyping *nga4-3*, PCR with primers SS065 and SS066 gave a 1-kb product for the wild-type allele, and PCR with primers SS065 and En8130 produced a 0.4-kb fragment for the mutant allele.

sty1-1 and *sty2-1* genotyping was performed as previously described (Kuusk et al., 2002).

Accession Numbers

Sequence data from this article can be found in the Arabidopsis Genome Initiative (AGI) or GenBank/EMBL data libraries under the following accession numbers: for *NGA1* to *NGA4*, the AGI numbers are At2g46870, At3g61970, At1g01030, and At4g01500, respectively. STY1, STY2, YUC1, YUC2, YUC4, and UBC21 correspond to At3g51060, At4g36260, At4g32540, At4g13260, At5g11320, and At5g25760, respectively. The GenBank number for the *laaL* sequence is M35373.

Supplemental Data

The following materials are available in the online version of this article.

Supplemental Figure 1. Description of the Alleles Used in This Study.

Supplemental Figure 2. Preanthesis Gynoecium Phenotypes of *nga3-3* Single Mutants.

Supplemental Figure 3. Fruit Phenotypes Caused by Overexpression of the NGA Genes and Leaf Phenotypes Caused by NGA Loss of Function.

Supplemental Figure 4. Design of the amiR-NGA Transgene and Effect in NGA Expression.

Supplemental Figure 5. Expression of NGA Genes in Different Tissues.

Supplemental Figure 6. Auxin-Related Phenotypes in *nga* Mutants.

Supplemental Figure 7. Phenotype of *nga3 nga4 sty1* Fruits.

Supplemental Figure 8. Multiple Alignment of C-t Domains of NGA Homologs and Phylogenetic Relationships of These Factors.

Supplemental Figure 9. Expression of YUC4_{PRO}:GUS in 35S_{PRO}:NGA3 Flowers.

Supplemental Table 1. Primers Used in This Work.

Supplemental Data Set 1. Text File of the Alignment Used to Generate the Phylogentic Tree Shown in Supplemental Figure 7.

ACKNOWLEDGMENTS

We thank Desmond Bradley, Francisco Madueño, and members of the Ferrándiz lab for critical reading of the manuscript and helpful comments and suggestions; Eva Sundberg and Yunde Zhao for providing seeds; and Rebecca Schwab for help in amiRNA design. Our work is supported by Research Grants BIO2002-01301 and BIO2005-01541 from the Ministerio de Educación y Ciencia of Spain to C.F. and BFU2006-00771 to S.P. and by grants from the National Science Foundation to M.Y. and D.W., and from the Max Planck Society to D.W. M.N.-G. and M.T. are supported by doctoral fellowships of the Generalitat Valenciana.

Received January 8, 2009; revised March 31, 2009; accepted April 23, 2009; published May 12, 2009.

REFERENCES

- Aloni, R., Aloni, E., Langhans, M., and Ullrich, C.I. (2006). Role of auxin in regulating Arabidopsis flower development. *Planta* **223**: 315–328.
- Aloni, R., Schwalm, K., Langhans, M., and Ullrich, C.I. (2003). Gradual shifts in sites of free-auxin production during leaf-primordium development and their role in vascular differentiation and leaf morphogenesis in Arabidopsis. *Planta* **216**: 841–853.
- Alonso-Cantabrana, H., Ripoll, J.J., Ochando, I., Vera, A., Ferrandiz, C., and Martinez-Laborda, A. (2007). Common regulatory networks in leaf and fruit patterning revealed by mutations in the Arabidopsis ASYMMETRIC LEAVES1 gene. *Development* **134**: 2663–2671.
- Alvarez, J., and Smyth, D. (1999). CRABS CLAW and SPATULA, two Arabidopsis genes that control carpel development in parallel with AGAMOUS. *Development* **126**: 2377–2386.
- Alvarez, J.P., Pekker, I., Goldshmidt, A., Blum, E., Amsellem, Z., and Eshed, Y. (2006). Endogenous and synthetic microRNAs stimulate simultaneous, efficient, and localized regulation of multiple targets in diverse species. *Plant Cell* **18**: 1134–1151.
- Balanza, V., Navarrete, M., Trigueros, M., and Ferrandiz, C. (2006). Patterning the female side of Arabidopsis: the importance of hormones. *J. Exp. Bot.* **57**: 3457–3469.
- Baumann, E., Lewald, J., Saedler, H., Schulz, B., and Wisman, E. (1998). Successful PCR-based reverse genetic screens using an En-1-mutagenised *Arabidopsis thaliana* population generated via single-seed descent. *Theor. Appl. Genet.* **97**: 729–734.
- Bennett, S.R.M., Alvarez, J., Bossinger, G., and Smyth, D.R. (1995). Morphogenesis in *pinoid* mutants of *Arabidopsis thaliana*. *Plant J.* **8**: 505–520.
- Blanc, G., and Wolfe, K.H. (2004). Functional divergence of duplicated genes formed by polyploidy during Arabidopsis evolution. *Plant Cell* **16**: 1679–1691.
- Blanc, G., Hokamp, K., and Wolfe, K.H. (2003). A recent polyploidy superimposed on older large-scale duplications in the Arabidopsis genome. *Genome Res.* **13**: 137–144.
- Bowman, J., and Smyth, D. (1999). CRABS CLAW, a gene that regulates carpel and nectary development in Arabidopsis, encodes a novel protein with zinc finger and helix-loop-helix domains. *Development* **126**: 2387–2396.
- Cheng, Y., Dai, X., and Zhao, Y. (2006). Auxin biosynthesis by the YUCCA flavin monooxygenases controls the formation of floral organs and vascular tissues in Arabidopsis. *Genes Dev.* **20**: 1790–1799.
- Cheng, Y., Dai, X., and Zhao, Y. (2007). Auxin synthesized by the YUCCA flavin monooxygenases is essential for embryogenesis and leaf formation in Arabidopsis. *Plant Cell* **19**: 2430–2439.
- Dinneny, J.R., and Yanofsky, M.F. (2005). Drawing lines and borders: How the dehiscent fruit of Arabidopsis is patterned. *Bioessays* **27**: 42–49.
- Ferrándiz, C., Gu, Q., Martienssen, R., and Yanofsky, M. (2000). Redundant regulation of meristem identity and plant architecture by FRUITFULL, APETALA1 and CAULIFLOWER. *Development* **127**: 725–734.
- Ferrándiz, C., Pelaz, S., and Yanofsky, M.F. (1999). Control of carpel and fruit development in Arabidopsis. *Annu. Rev. Biochem.* **68**: 321–354.
- Gremski, K., Ditta, G., and Yanofsky, M.F. (2007). The HECATE genes regulate female reproductive tract development in *Arabidopsis thaliana*. *Development* **134**: 3593–3601.
- Groszmann, M., Paicu, T., and Smyth, D.R. (2008). Functional domains of SPATULA, a bHLH transcription factor involved in carpel and fruit development in Arabidopsis. *Plant J.* **55**: 40–52.
- Heisler, M., Atkinson, A., Bylstra, Y., Walsh, R., and Smyth, D. (2001). SPATULA, a gene that controls development of carpel margin tissues in Arabidopsis, encodes a bHLH protein. *Development* **128**: 1089–1098.
- Hobbie, L., McGovern, M., Hurwitz, L., Pierro, A., Liu, N., Bandyopadhyay, A., and Estelle, M. (2000). The *axr6* mutants of *Arabidopsis thaliana* define a gene involved in auxin response and early development. *Development* **127**: 23–32.
- Jensen, P.J., Hangarter, R.P., and Estelle, M. (1998). Auxin transport is required for hypocotyl elongation in light-grown but not dark-grown Arabidopsis. *Plant Physiol.* **116**: 455–462.
- Kim, J.I., et al. (2007). *yucca6*, a dominant mutation in Arabidopsis, affects auxin accumulation and auxin-related phenotypes. *Plant Physiol.* **145**: 722–735.
- Kuusk, S., Sohlberg, J.J., Long, J.A., Fridborg, I., and Sundberg, E. (2002). STY1 and STY2 promote the formation of apical tissues during Arabidopsis gynoecium development. *Development* **129**: 4707–4717.
- Kuusk, S., Sohlberg, J.J., Magnus Eklund, D., and Sundberg, E. (2006). Functionally redundant SHI family genes regulate Arabidopsis gynoecium development in a dose-dependent manner. *Plant J.* **47**: 99–111.
- Liljgren, S.J., Roeder, A.H., Kempin, S.A., Gremski, K., Ostergaard, L., Guimil, S., Reyes, D.K., and Yanofsky, M.F. (2004). Control of fruit patterning in Arabidopsis by INDEHISCENT. *Cell* **116**: 843–853.
- Marsch-Martinez, N., Greco, R., Van Arkel, G., Herrera-Estrella, L., and Pereira, A. (2002). Activation tagging using the En-1 maize transposon system in Arabidopsis. *Plant Physiol.* **129**: 1544–1556.
- Nemhauser, J., Feldman, L., and Zambryski, P. (2000). Auxin and ETTIN in Arabidopsis gynoecium morphogenesis. *Development* **127**: 3877–3888.
- Okada, K., Ueda, J., Komaki, M.K., Bell, C.J., and Shimura, Y. (1991). Requirement of the auxin polar transport system in early stages of *Arabidopsis* floral bud formation. *Plant Cell* **3**: 677–684.
- Pekker, I., Alvarez, J.P., and Eshed, Y. (2005). Auxin response factors

- mediate *Arabidopsis* organ asymmetry via modulation of KANADI activity. *Plant Cell* **17**: 2899–2910.
- Reinhardt, D.** (2003). Vascular patterning: More than just auxin? *Curr. Biol.* **13**: R485–R487.
- Robles, P., and Pelaz, S.** (2005). Flower and fruit development in *Arabidopsis thaliana*. *Int. J. Dev. Biol.* **49**: 633–643.
- Romano, C.P., Robson, P.R., Smith, H., Estelle, M., and Klee, H.** (1995). Transgene-mediated auxin overproduction in *Arabidopsis*: Hypocotyl elongation phenotype and interactions with the *hy6-1* hypocotyl elongation and *axr1* auxin-resistant mutants. *Plant Mol. Biol.* **27**: 1071–1083.
- Schmid, M., Davison, T.S., Henz, S.R., Pape, U.J., Demar, M., Vingron, M., Scholkopf, B., Weigel, D., and Lohmann, J.U.** (2005). A gene expression map of *Arabidopsis thaliana* development. *Nat. Genet.* **37**: 501–506.
- Schwab, R., Ossowski, S., Riester, M., Warthmann, N., and Weigel, D.** (2006). Highly specific gene silencing by artificial microRNAs in *Arabidopsis*. *Plant Cell* **18**: 1121–1133.
- Sessions, A., et al.** (2002). A high-throughput *Arabidopsis* reverse genetics system. *Plant Cell* **14**: 2985–2994.
- Sessions, A., Nemhauser, J., McColl, A., Roe, J., Feldmann, K., and Zambryski, P.** (1997). *ETTIN* patterns the *Arabidopsis* floral meristem and reproductive organs. *Development* **124**: 4481–4491.
- Sessions, R.A., and Zambryski, P.C.** (1995). *Arabidopsis* gynoecium structure in the wild type and in *ettin* mutants. *Development* **121**: 1519–1532.
- Sohlberg, J.J., Myrenas, M., Kuusk, S., Lagercrantz, U., Kowalczyk, M., Sandberg, G., and Sundberg, E.** (2006). STY1 regulates auxin homeostasis and affects apical-basal patterning of the *Arabidopsis* gynoecium. *Plant J.* **47**: 112–123.
- Staldal, V., Sohlberg, J.J., Eklund, D.M., Ljung, K., and Sundberg, E.** (2008). Auxin can act independently of CRC, LUG, SEU, SPT and STY1 in style development but not apical-basal patterning of the *Arabidopsis* gynoecium. *New Phytol.* **180**: 798–808.
- Swaminathan, K., Peterson, K., and Jack, T.** (2008). The plant B3 superfamily. *Trends Plant Sci.* **13**: 647–655.
- Timpte, C., Lincoln, C., Pickett, F.B., Turner, J., and Estelle, M.** (1995). The AXR1 and AUX1 genes of *Arabidopsis* function in separate auxin-response pathways. *Plant J.* **8**: 561–569.
- Weigel, D., et al.** (2000). Activation tagging in *Arabidopsis*. *Plant Physiol.* **122**: 1003–1013.
- Weigel, D., and Glazebrook, J.** (2002). *Arabidopsis: A Laboratory Manual*. (Cold Spring Harbor, NY: Cold Spring Harbor Laboratory Press).
- Wisman, E., Cardon, G.H., Fransz, P., and Saedler, H.** (1998). The behaviour of the autonomous maize transposable element *En/Spm* in *Arabidopsis thaliana* allows efficient mutagenesis. *Plant Mol. Biol.* **37**: 989–999.
- Woodward, C., Bemis, S.M., Hill, E.J., Sawa, S., Koshiba, T., and Torii, K.U.** (2005). Interaction of auxin and ERECTA in elaborating *Arabidopsis* inflorescence architecture revealed by the activation tagging of a new member of the YUCCA family putative flavin monooxygenases. *Plant Physiol.* **139**: 192–203.
- Zhao, Y., Christensen, S.K., Fankhauser, C., Cashman, J.R., Cohen, J.D., Weigel, D., and Chory, J.** (2001). A role for flavin monooxygenase-like enzymes in auxin biosynthesis. *Science* **291**: 306–309.

The NGATHA Genes Direct Style Development in the Arabidopsis Gynoecium

Marina Trigueros, Marisa Navarrete-Gómez, Shusei Sato, Sioux K. Christensen, Soraya Pelaz, Detlef Weigel, Martin F. Yanofsky and Cristina Ferrándiz
PLANT CELL 2009;21;1394-1409; originally published online May 12, 2009;
DOI: 10.1105/tpc.109.065508

This information is current as of October 29, 2010

Supplemental Data	http://www.plantcell.org/cgi/content/full/tpc.109.065508/DC1
References	This article cites 45 articles, 26 of which you can access for free at: http://www.plantcell.org/cgi/content/full/21/5/1394#BIBL
Permissions	https://www.copyright.com/ccc/openurl.do?sid=pd_hw1532298X&issn=1532298X&WT.mc_id=pd_hw1532298X
eTOCs	Sign up for eTOCs for <i>THE PLANT CELL</i> at: http://www.plantcell.org/subscriptions/etoc.shtml
CiteTrack Alerts	Sign up for CiteTrack Alerts for <i>Plant Cell</i> at: http://www.plantcell.org/cgi/alerts/ctmain
Subscription Information	Subscription information for <i>The Plant Cell</i> and <i>Plant Physiology</i> is available at: http://www.aspb.org/publications/subscriptions.cfm

© American Society of Plant Biologists

ADVANCING THE SCIENCE OF PLANT BIOLOGY